IEEE Access
Multidisciplinary | Rapid Review | Open Access Journal

Received September 1, 2018, accepted September 23, 2018, date of publication October 2, 2018, date of current version October 25, 2018.

Digital Object Identifier 10.1109/ACCESS.2018.2873174

A Topographic Kirchhoff Dynamic Focused Beam Migration Method Based on Compressed Sensing

HUI SUN[1,2,3], FEILONG YANG[4], FANCHANG MENG[5], ZHIHOU ZHANG[1,2], CHENG GAO[6], AND MINGCHEN LIU[7]

[1]Faculty of Geosciences and Environmental Engineering, Southwest Jiaotong University, Chengdu 611756, China
[2]MOE Key Laboratory of High-speed Railway Engineering, Southwest Jiaotong University, Chengdu 610031, China
[3]School of Resources and Environment, University of Electronic Science and Technology of China, Chengdu 611731, China
[4]School of Earth Sciences and Engineering, Xi'an Shiyou University, Xi'an 710065, China
[5]Institute of Geology and Geophysics, The Chinese Academy of Sciences, Beijing 100029, China
[6]School of Mines, Inner Mongolia University of Technology, Hohhot 010051, China
[7]College for Geoexploration Science Technology, Jilin University, Changchun 130026, China

Corresponding author: Feilong Yang (feilongy@xsyu.edu.cn)

This work was supported in part by the Natural Science Foundation of China under Grant 41804100, in part by the Fundamental Research Funds for the Central Universities under Grant A0920502051820-36, in part by the Science Research Project of Inner Mongolia University of Technology under Grant ZD201622, in part by the Science Research Project of Institutions of Higher Learning in Inner Mongolia under Grant NJZZ18079, in part by the Natural Science Foundation of Inner Mongolia under Grant 2018BS04002, and in part by the China Geological Survey Project under Grant 121201011000150013-05.

ABSTRACT Kirchhoff beam migration (KBM) is a ray-based seismic imaging method, which can handle multi-arrivals caused by model complexity. Apart from its high imaging precision, it also retains the merits of Kirchhoff migration, such as efficiency, stability, and flexibility. However, two issues should be taken into consideration when this method is expanded to the complicated surface conditions: first, the computational accuracy deficiency of the original local plane-wave decomposition method cannot suit for low signal-to-noise ratio seismic data; second, as the rays traveling, the beam width increases rapidly, which cannot guarantee the computational accuracy of the corresponding grid points' attribute information. In addition, the insufficient coverage of the beam in the shallow part of the model might affect the imaging quality of this region. Kirchhoff dynamic focused beam migration based on compressed sensing is proposed to resolve these two problems. For the first problem, the local plane-wave decomposition method based on compressed sensing is introduced into KBM to enhance its computational accuracy. To solve the second problem, this paper adopts the dynamic focused beam to replace the original simplified Gaussian beam in the migration method, control the divergence of beam, and increase the coverage of beam in the shallow part of the model. Both Marmousi model and Canadian Foothills model are employed in this paper to test the new migration imaging method.

INDEX TERMS Signal processing, compressive sensing (CS), seismic imaging method, Kirchhoff beam migration, dynamic focused beam.

I. INTRODUCTION

Prestack depth migration is an important seismic imaging method [1], which has a wide application in seismic prospecting [2]–[9] and can mainly be divided into two types, including ray-based methods and finite-difference methods [10]. Beam migration is a ray-based methods, in which seismic data panels are decomposed into plane waves at beam centers and every plane wave will be migrated in the algorithm [11]. So beam migration is able to handle multi-arrival energy, which make it to be an imaging method boasting the advantages of high accuracy and high efficiency [12].

Hill [13] (1990) put forward poststack Gaussian beam migration (GBM), which laid the theoretical foundations for beam migration. Several key issues were then discussed to improve the computational efficiency of poststack GBM [14], [15]. Even so, it is difficult to extend the method to the prestack case for its inefficiency. Hill [16] (2001) solved this problem by reducing the integration in the imaging formula with a saddle-point approximation approach and proposed the prestack depth Gaussian beam migration on common-offset gathers. To widen its application, prestack depth GBM was further adapted to a common-shot migration method by Nowack *et al.* [17] (2003) and Gray [18] (2005). Dip filtering was introduced into beam migration by Ting and Wang [19] (2009) and was successfully applied in Gulf of Mexico. Sherwood et al. (2009) proposed a beam

migration method based on wavelets, in which the recorded data is decomposed into a basic of wavelets and migrated by a ''point to point mapping'' approach. This method could easily be extended from a 2D case to a 3D case [20]. Gray and Bleistein (2009) proposed a true-amplitude GBM method [21], which introduced the true-amplitude theory into GBM [22], [23]. Popov *et al.* [24] (2010) presented the GBM summation method, which strictly follows the Kirchhoff migration principles. Compared with Hill's (2001) GBM, this method has higher accuracy but much lower computational efficiency, so it is usually used in oriented region imaging. The GBM summation method could also be used in born modeling for heterogeneous media [25]. Focusing on obtaining kinematic accuracy and computational efficiency, Kirchhoff beam migration (KBM) was proposed [26]. The mechanics of KBM are analogs to GBM except for ignoring the dynamic information and employing the simplified Gaussian beam to control the beam coverage. Then KBM was further developed for accommodating the common-shot data sets [27]. Delta packet was also used for calculating the Green's function, which is essential to beam migration [28], [29]. By adopting this method, GBM could be transformed into a time domain imaging method. In order to improve the traveltime calculation accuracy in the seismic imaging method, Sun et al. (2017) combined Wavefront Construction (WFC) and Fast Marching Method (FFM) to achieve a new traveltime calculation method [30]. Complex traveltime was also obtained by solving the complex eikonal equation [31]-[33].

Seismic explorations are often conducted in rugged topography. Gray [18] (2005) corrected the elevations of the receivers according to the beam center's elevation and proposed a common-shot topographic GBM. On the basis of this method, Yue *et al.* [34] (2010) also studied the topographic GBM. The local slant stacking formula in Yue's method is modified to obtain more accurate plane waves under topography and the migration results verify that this method can improve the imaging quality in the shallow part of Canadian Foothills model compared with Gray's method. Based on the same implementation strategy, true-amplitude GBM was adapted to suit for the rugged topography [35]. Wave field approximation in effective vicinity and Fresnel beam were also considered to combine with topographic true-amplitude GBM for improving its imaging quality [36].

Local plane wave decomposition is a critical step in beam migration, which has an important impact on beam migration methods' imaging abilities. Hu and Stoffa (2009) presented a slowness-driven GBM to remove the migration swing artifacts, which were generated from low-fold seismic data imaging. In this method, the coherency of a locally coherent seismic event is employed for calculating the weighting function, which is added to the imaging formula of GBM [37]. Yang et al. (2015) also used the local similarity analysis in local plane wave decomposition of GBM and proved it effective for low-fold data sets [38]. Introducing the least square inversion fashion into local slant stacking operator, Wu *et al.* (2014) proposed a high-resolution beam forming method for 3D common-offset KBM [39], which was also employed for velocity analysis [40]-[43]. Wu *et al.* [44] (2015) then applied the migration algorithm to image the SEAM model. Wang *et al.* [45] (2015) decomposed the plane waves under the framework of compressed sensing in the characteristic-wave imaging method. This decomposed method can sparely express the seismic data [46]. Liu *et al.* [47] (2015) further studied this characteristic-wave prestack depth migration and extended it to be an anisotropic medium imaging method. Sun *et al.* [48] (2018) incorporated compressive sensing technique into KBM to improve its imaging ability.

Beam propagator's effect to the imaging method received more and more attention in recent years. Conventional GBM adopted Gaussian beam [49] as its propagator, whose geometry is determined by dynamic ray-tracing parameters. If the initial beam width is small, the beam width will increase rapidly along with ray propagation. Employing the stationary-phase approximation to integral of Kirchhoff migration's imaging formula, Sun and Schuster [50] (2001) succeed in controlling the imaging region and obtaining more clearer migration images. Nowack [51] (2008) used focused Gaussian beam in GBM, which actually is a transformed Gaussian beam. Focused Gaussian beam can flexibly control the narrowest part of the beam to occur at the target location. Nowack [52] (2011) further studied the focused Gaussian beam and transformed it to a dynamic focused beam and proposed a dynamically focused Gaussian beam migration algorithm. The dynamic focused beam can control beam width along all the ray path. Yang *et al.* [53] (2015) introduced also studied the dynamically focused Gaussian beam migration and extended it to a true-amplitude seismic imaging method. Analogous to focused beam, laser beam also can control the geometry of the beam and was respectively applied to viscoelastic medium beam migration [54] and anisotropic medium beam migration [55]. Huang *et al.* [56] (2015) adopted Fresnel beam to control the shape of the beam by combining the concept of Fresnel zone with the wave field approximation theory. A common-shot Fresnel beam migration method was presented and extended to suit for the complex topography.

This paper studies the KBM under irregular topography. Two improvements are made to improve the imaging ability of KBM. Key steps of CS-KDFBM including imaging principle, local plane-wave decomposition method and dynamic focused beam propagator will be stated in the next part. Marmousi model and Canadian Foothills model will be employed to test the new method.

II. METHODS

The common-shot migration formula of KBM can be summarized as [27]:

$$I_s(\mathrm{x}) = \sum_{L_r} \int dp_s \int dp_r A \cdot D_s(L, p', \tau') \qquad (1)$$

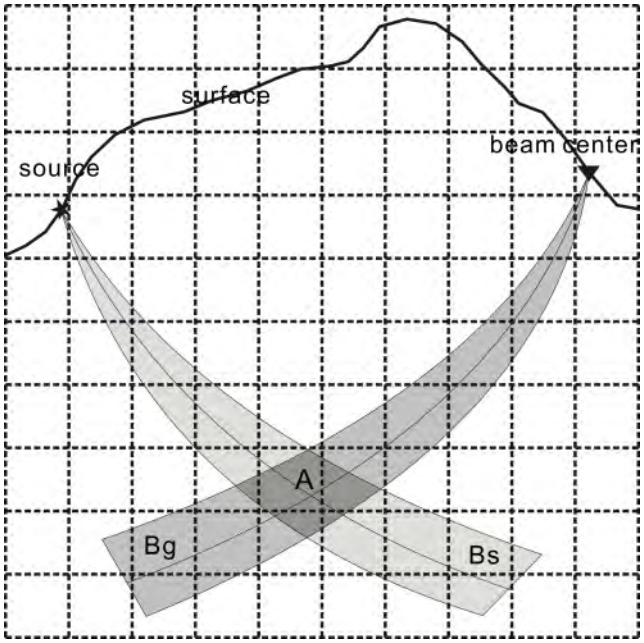

FIGURE 1. Schematic diagram of the imaging region, Bs represents the beam emitted from the source, Bg represents the beam emitted from beam center, the overlap region A is the computational area. Time shift calculation under complex topographic condition, asterisk represents beam center; inverted triangle represents receiver.

Where x is the imaging node; I_s is the migration result of single shot; L_r is the window; p_s is the slowness of rays emitted from the source; p_r is the slowness of rays emitted from the beam centers; A is the weight function; p' is the local plane waves decomposed from the original seismic data. The imaging conditions of the migration formula are:

$$\tau' = t_s + t_g \tag{2}$$

$$p' = p_r \tag{3}$$

Where t_s and t_g respectively denote traveltime from the target points to the source and beam center. The expression of the migration formula is an integral of the beams. Every pair of the beams will be migrated and only the overlap regions will be calculated (See Fig. 1).

A. LOCAL PLANE WAVE DECOMPOSITION

To image the subsurface nodes, it is required to decompose the seismic records into plane waves. Conventional beam migration methods employed linear radon transform (LRT) to finish this task.

The seismic records of every window need to be decomposed into plane waves in KBM. The expressions of seismic record $\boldsymbol{D}(\omega)$ and plane-wave result $\boldsymbol{P}(\omega)$ are:

$$\boldsymbol{D}(\omega) = [x_1(\omega), x_2(\omega), \cdots, x_{nx}(\omega)]^{\mathrm{T}} \tag{4}$$

$$\boldsymbol{P}(\omega) = [p_1(\omega), p_2(\omega), \cdots, p_{np}(\omega)]^{\mathrm{T}} \tag{5}$$

where, nx is the number of traces; np is the number of slowness samples; $x_1(\omega) \sim x_{nx}(\omega)$ is the records; $p_1(\omega) \sim p_{nx}(\omega)$ is the plane wave data. In CS-LRT, the minimized target function is established as:

$$\boldsymbol{J} = \|\boldsymbol{D}(\omega) - \boldsymbol{L}(\omega)\boldsymbol{P}(\omega)\|^2 + \|\boldsymbol{W_P}(\omega)\boldsymbol{P}(\omega)\|^2 \tag{6}$$

where, $\boldsymbol{W_P}(\omega)$ is the space weighted matrix, $\boldsymbol{L}(\omega)$ is the operator matrix. Set $\boldsymbol{P}(\omega)$ to 0 and we can obtain the solution:

$$\boldsymbol{P}(\omega) = [\boldsymbol{L}^{\mathbf{H}}(\omega)\boldsymbol{L}(\omega) + \boldsymbol{W}_{\boldsymbol{P}}^{-1}(\omega)]^{-1}\boldsymbol{L}^{\mathbf{H}}(\omega)\boldsymbol{D}(\omega) \tag{7}$$

The plane-wave decomposition is expressed as:

$$\begin{aligned} &\min \ \|\boldsymbol{P}(\omega)\|_0^0, \\ &S.T. \ \|\boldsymbol{D}(\omega) - \boldsymbol{L}(\omega)\boldsymbol{P}(\omega)\|_2^2 < \varepsilon \end{aligned} \tag{8}$$

where, ε is the noise of the target data. Then we can obtain the high-quality plane-wave data by employing the CS-LRT.

Decomposing the seismic data under irregular topography is different from that of horizontal surface. In this case, not only the horizontal distance between receiver and beam center but also their difference of height has effect on the time shift in CS-LRT. The way to calculate the time shift under irregular topography is shown below.

In Fig.2, the height of beam center is marked as 0 and the horizontal location of beam center is L. The receiver has a height of h and a horizontal location of x_r. The slowness of plane waves at beam center is p_L. Time shift of the receiver is described as:

$$\begin{aligned} \Delta\tau &= \frac{d_{x_rL} + d_{h0}}{V_{(L,0)}} = \frac{(x_r - L) * \sin\theta + h * \cos\theta}{V_{(L,0)}} \\ &= p_{Lx}(x_r - L) + p_{Lz}h \end{aligned} \tag{9}$$

Where p_{Lx} and p_{Lz} are, respectively, the horizontal and vertical component of slowness.

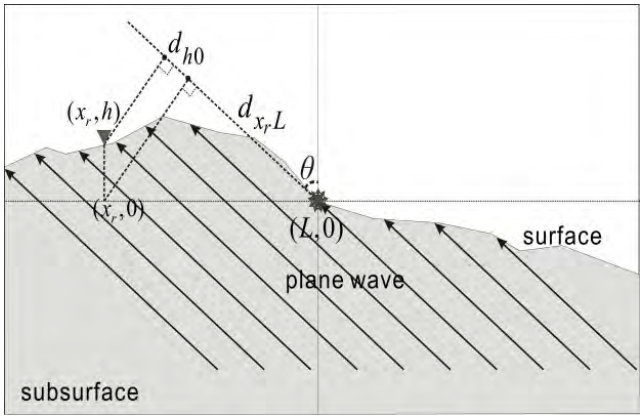

FIGURE 2. Time shift calculation under complex topographic condition, asterisk represents beam center; inverted triangle represents receiver.

B. BEAM PROPAGATOR

The final image of KBM is acquired by adding the imaging result of all pairs of beams together. Beam propagator can influence the imaging ability of beam migration from the aspects of imaging accuracy and computational efficiency.

Dynamic focused beam is essentially the special form of Gaussian beam, whose theoretical basis is the high frequency approximate solution of the wave equation:

$$u(s, n, \omega) = \sqrt{\frac{V(s)}{Q(s)}} \exp\left\{ i\omega\tau(s) + \frac{i\omega}{2}\frac{P(s)}{Q(s)}n^2 \right\} \tag{10}$$

where, s and n are the ray-centered coordinates; ω is the frequency; u is the value of wave field; V is the velocity; $\tau(s)$ is the traveltime along the central ray; $P(s)$ and $Q(s)$ are dynamic ray parameters, which are obtained by solving the dynamic ray equations [57]:

$$\begin{cases} \dfrac{d}{d\tau}\mathbf{Q} = v^2\mathbf{P} \\ \dfrac{d}{d\tau}\mathbf{P} = v^{-1}\mathbf{V}\mathbf{Q} \end{cases} \tag{11}$$

$\mathbf{Q}$, $\mathbf{P}$ and $\mathbf{V}$ are all 2×2 matrices. To ensure (13) is the expression of Gaussian beam, two conditions need to be satisfied: one is that the value of dynamic ray parameters must be complex and another is Im($\mathbf{P}/\mathbf{Q}$) should be greater than zero. In this case, the solutions of wave equation can concentrate close to the central ray. Normally, two methods including the direct method and indirect methods were adopted to solve the dynamic ray tracing systems. The direct method solves the equations by using the appropriate complex initial value, which was adopted by conventional GBM [13], [16]. The indirect method first solves the equations to obtain real matrices, and then the real matrices are multiplied by the constant complex coefficient to acquire the complex results. Dynamic focused beam employs the indirect method to solve the dynamic ray tracing systems. The fundamental matrix of real solutions of (11) can be expressed as:

$$\pi(s) = \begin{pmatrix} q_1(s) & q_2(s) \\ p_1(s) & p_2(s) \end{pmatrix} \tag{12}$$

The constant complex coefficients are z_1 and z_2. Complex solutions of (11) are:

$$\begin{pmatrix} q(s) \\ p(s) \end{pmatrix} = \pi(s)\begin{pmatrix} z_1 \\ z_2 \end{pmatrix} = \begin{pmatrix} z_1q_1(s) + z_2q_2(s) \\ z_1p_1(s) + z_2p_2(s) \end{pmatrix} \tag{13}$$

Introduce a new complex coefficient $\varepsilon = z_1/z_2$, $p(s)/q(s)$ is

$$\frac{p(s)}{q(s)} = \frac{\varepsilon p_1(s) + p_2(s)}{\varepsilon q_1(s) + q_2(s)} \tag{14}$$

$\varepsilon$is a constant in conventional Gaussian beam, while in dynamic focused beam, ε is a variable and can be expressed as:

$$\varepsilon(s) = \frac{-q_2(s) - i\omega_{ref}l^2(s)p_2(s)}{q_1(s) + i\omega_{ref}l^2(s)p_s(s)} \tag{15}$$

Where ω_{ref} is the reference frequency. The expression of $l(s)$ is

$$l(s) = \frac{2\pi v(s)}{\omega_{ref}} \tag{16}$$

Fig. 3 is the comparison diagram of beam geometry in Marmousi model. Fig. 3a and Fig. 3b are, respectively, the geometry of Gaussian beam and dynamic focused beam. Both the two beams have the same start point at the location (3500 m, 4 m); the same launch direction of 15°; the same frequency of 15 Hz; the same reference frequency of 10 Hz; and the same initial beam width of 200 m. It can be seen that the width of Gaussian beam increases rapidly with the ray propagating and the dynamic focused beam can control the beam width well. The reason is that Gaussian beam employed the constant ε in (14), as the beam travels, it will diverge and the beam width will also increase. Dynamic focused beam adopted a variable εin (14), the amount of change in ε is to eliminate the change in beam width.

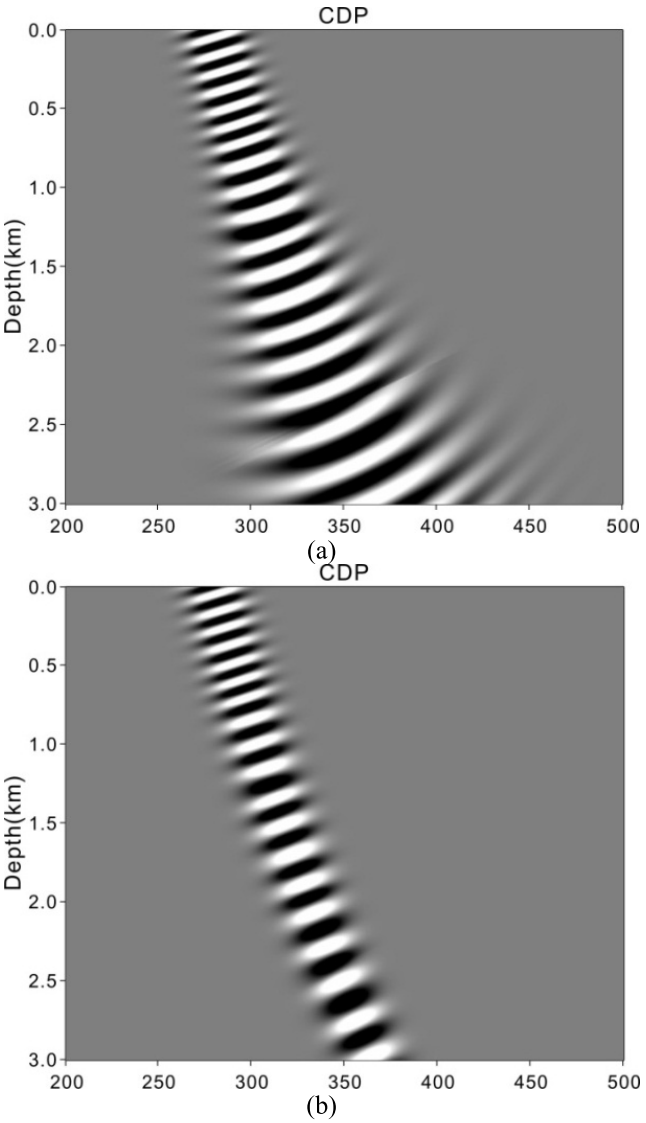

FIGURE 3. Comparison diagram of beam geometry in Marmousi model, (a) geometry of Gaussian beam, (b) geometry of dynamic focused beam.

C. TRAVELTIME CALCULATION

Traveltime is also an important seismic attribute information, which has great influence on migration imaging. The grid

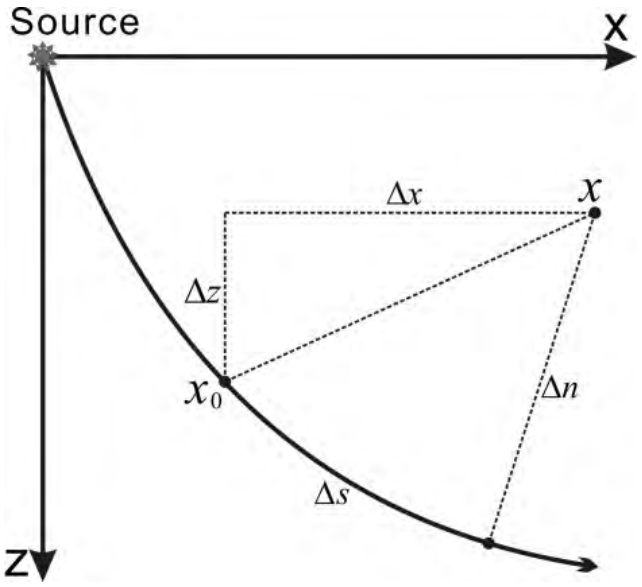

FIGURE 4. Schematic diagram of traveltime extrapolation.

nodes' traveltime within the beam is extrapolation from the information of their nearest discrete nodes in the central rays. Traveltime calculation mainly consists of two main steps: central ray tracing and travel time extrapolation. These two steps are not affected by topographic surface during the calculation. So, this derivation is carried out under the horizontal surface.

As is shown in Fig. 4, $\boldsymbol{x}$ is the grid node within the beam; $\boldsymbol{x}_0$ is the discrete node, which is nearest to $\boldsymbol{x}$ in the central ray. The distance differences between the two points in Cartesian coordinates are Δx along the x direction and Δz along the z direction; in ray-centered coordinates are Δs along the ray path and Δn perpendicular from the ray path; $T(\boldsymbol{x}_0)$ and $T(\boldsymbol{x})$ are, respectively, the traveltime of $\boldsymbol{x}$ and $\boldsymbol{x}_0$; Taylor's approximation expression of $T(\boldsymbol{x}_0)$ is

$$T(\boldsymbol{x}) \approx T(\boldsymbol{x}_0) + T(\boldsymbol{x})' + \frac{1}{2}T(\boldsymbol{x})'' \tag{17}$$

The first and second derivatives of the $T(\boldsymbol{x})$ in the ray-centered coordinates are respectively $T(\boldsymbol{x})'$ and $T(\boldsymbol{x})''$. The expression of $T(\boldsymbol{x})'$ is

$$\begin{aligned} T'(\boldsymbol{x}) &= \left(\Delta x\frac{\partial}{\partial x} + \Delta z\frac{\partial}{\partial z}\right)T\Big|_{T=T(s,n)} \\ &= \Delta x p_x + \Delta z p_z \end{aligned} \tag{18}$$

p_x and p_z are the components of slowness in the x and z direction. The expression of $T(\boldsymbol{x})''$ is

$$\begin{aligned} T''(\boldsymbol{x}) &= \left(\Delta s\frac{\partial}{\partial s} + \Delta n\frac{\partial}{\partial n}\right)^2 T\Big|_{T=T(s,n)} \\ &= \left\{\Delta^2 s\left(-\frac{1}{v^2(s,n)}\frac{\partial v}{\partial s}\right) + 2\Delta s\Delta n\left(-\frac{1}{v^2(s,n)}\frac{\partial v}{\partial n}\right)\right. \\ &\quad \left. + \Delta^2 n\frac{\partial^2 T}{\partial n^2}\right\}\Big|_{T=T(s,n)} \end{aligned} \tag{19}$$

Where v represents the velocity; θ represents the ray direction; Consider the transformation between the Cartesian coordinates and the ray-centered coordinates

$$\begin{cases} \Delta s = \sin\theta\Delta x + \cos\theta\Delta z \\ \Delta n = \cos\theta\Delta x - \sin\theta\Delta z \end{cases} \tag{20}$$

(19) can be further expressed as

$$\begin{aligned} T''(\boldsymbol{x}) = \Big\{&(\sin\theta\Delta x + \cos\theta\Delta z)^2 \\ &* \left(-\frac{1}{v^2(s,n)}\left(\frac{\partial v}{\partial x}\sin\theta + \frac{\partial v}{\partial z}\cos\theta\right)\Big|_{v=v(s,n)}\right) \\ &+ 2(\sin\theta\Delta x + \cos\theta\Delta z)(\cos\theta\Delta x - \sin\theta\Delta z) \\ &\times \left(-\frac{1}{v^2(s,n)}\left(\frac{\partial v}{\partial x}\cos\theta - \frac{\partial v}{\partial z}\sin\theta\right)\Big|_{v=v(s,n)}\right) \\ &+ (\cos\theta\Delta x - \sin\theta\Delta z)^2\frac{\partial^2 T}{\partial n^2}\Big|_{T=T(s,n)}\Big\} \end{aligned} \tag{21}$$

Then,the traveltime of $\boldsymbol{x}$ is

$$\begin{aligned} T(\boldsymbol{x}) &= T(x+\Delta x, z+\Delta z) \\ &= T(x,z) + \Delta x p_x + \Delta z p_z \\ &\quad + \frac{1}{2}\Delta^2 x\Big(-p_x^2\left(\frac{\partial v}{\partial x}\sin\theta + \frac{\partial v}{\partial z}\cos\theta\right) \\ &\quad - 2p_x p_z\left(\frac{\partial v}{\partial x}\cos\theta - \frac{\partial v}{\partial z}\sin\theta\right) \\ &\quad + p_z^2 v^2(x,z)\frac{\partial^2 T}{\partial n^2}\Big)\Big|_{T=T(x,z)} \\ &\quad + \Delta x\Delta z\Big(p_x^2\left(\frac{\partial v}{\partial x}\cos\theta - \frac{\partial v}{\partial z}\sin\theta\right) \\ &\quad - p_x p_{zz}\Big(\left(\frac{\partial v}{\partial x}\sin\theta + \frac{\partial v}{\partial z}\cos\theta\right) + v^2(x,z)\frac{\partial^2 T}{\partial n^2}\Big) \\ &\quad - \left(p_z^2\frac{\partial v}{\partial x}\cos\theta - \frac{\partial v}{\partial z}\sin\theta\right)\Big)\Big|_{T=T(x,z)} \\ &\quad + \frac{1}{2}\Delta^2 z\Big(p_x^2 v^2(x,z)\frac{\partial^2 T}{\partial n^2} \\ &\quad + 2p_x p_z\left(\frac{\partial v}{\partial x}\cos\theta - \frac{\partial v}{\partial z}\sin\theta\right) \\ &\quad - p_z^2\left(\frac{\partial v}{\partial x}\sin\theta + \frac{\partial v}{\partial z}\cos\theta\right)\Big)\Big|_{T=T(x,z)} \end{aligned} \tag{22}$$

D. AMPLITUDE CALCULATION

KBM is a beam prestack depth migration method focusing on obtaining high computational efficiency, whose requirements for amplitude information are not as accurate as other beam migration methods. The calculation principle of its weight function is relatively simple, namely, the closer to the central ray, the larger the weight function. The principle is selected based on two considerations. Firstly, the beam energy is attenuated from the central ray to the sides, and the closer to the central ray, the larger the amplitude; Second, grid nodes' traveltime is calculated by the Taylor's approximation,

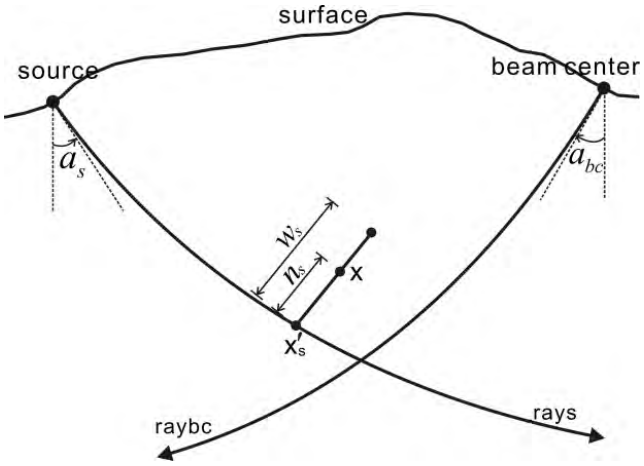

FIGURE 5. Schematic diagram of traveltime extrapolation.

and the closer to the central ray, the smaller the relative error, the larger the weight function should be. In this paper, the weight function calculation method is based on the original method [26], which will be introduced first.

As is shown in Fig. 5, rays is the ray emitted from the source and the angle between its initial direction and the vertical direction is a_s; raybc is the ray emitted from the beam center and the angle between its initial direction and the vertical direction is a_{bc}; x is the imaging point and its projection point on rays is x'$_s$; The distance between x and x'$_s$ is n_s; The width of rays at x'$_s$ is w_s; The distance between X and its projection point on raybc is n_{bc}; The width of rays at the projection point of x is w_s; The weight function of x can be described as:

$$A = \cos^2\left[\frac{\pi}{4}\left(n_s^2 w_s^{-2} + n_{bc}^2 w_{bc}^{-2}\right)\right]\cos\left[0.5 * (a_s - a_{bc})\right] \tag{23}$$

Adding the term $\cos[0.5 * (a_s - a_{bc})]$ is to weaken the effect of wide-angle post-critical energy to the migration method.

In (23), the beam width corresponding to a certain point on the central ray can be calculated, which cannot be achieved in the calculation of dynamic focused beam. So this formula is not suitable for CS-KDFBM and we need to find new parameter to replace the distance parameter.

In the previous section, we introduce the traveltime calculation method. The traveltime obtained by using (22) is complex, whose imaginary part is related to the amplitude attenuation of the beam. The larger the absolute value of the imaginary part, the smaller the beam amplitude is. This parameter can also reflect the distance between the target and the central ray. We employ the imaginary part of traveltime to replace the distance parameter in CS-KDFBM. Dynamic focused beam is realized by a recursive algorithm, in which a critical value of imaginary part of the traveltime is defined. When the calculated value exceeds the critical value, the recursive operation will be stopped. This critical

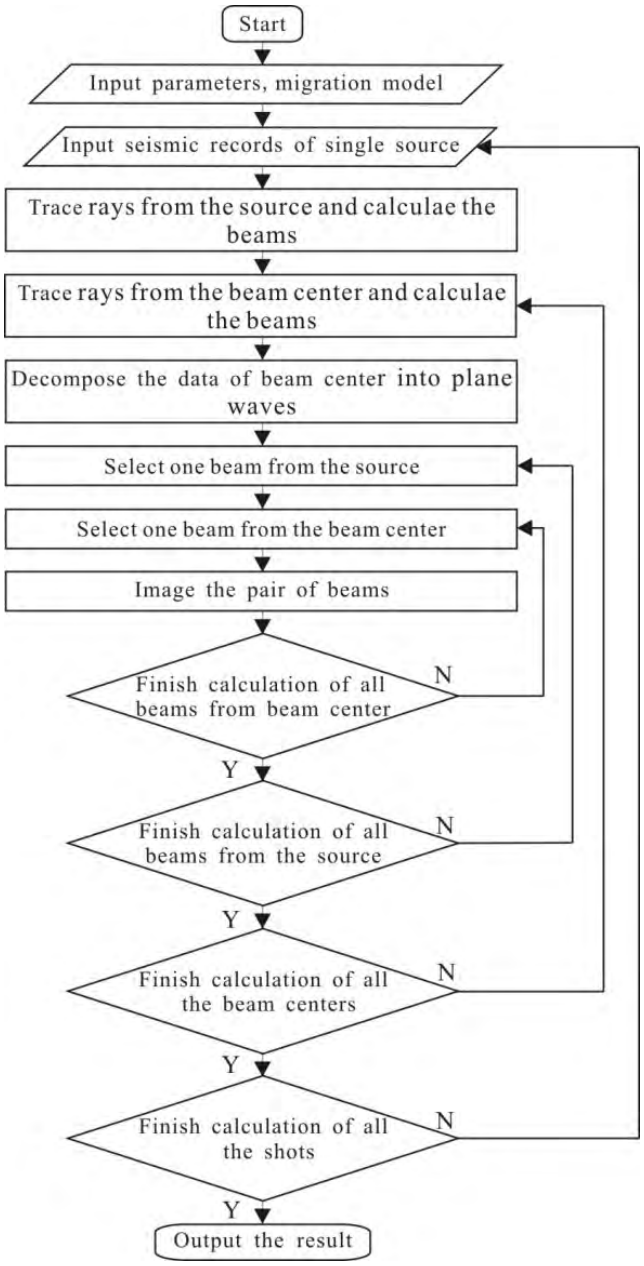

FIGURE 6. Implementing flow chart of CS-KDFBM.

value is used to replace the beam width of the central ray. The new amplitude calculation formula in CS-KDFBM can be obtained by referring to (23)

$$A = \cos^2\left[\frac{\pi}{4}\left(\tau_{is}^2 \tau_{imax}^{-2} + \tau_{ibc}^2 \tau_{imax}^{-2}\right)\right]\cos\left[0.5 * (a_s - a_{bc})\right] \tag{24}$$

Where τ_{is} is the imaginary part of traveltime from rays; τ_{ibc} is the imaginary part of traveltime from raybc; τ_{imax} is the defined critical value.

E. PROCESSING FLOW

The calculation flow of CS-KDFBM is shown in Fig. 6:

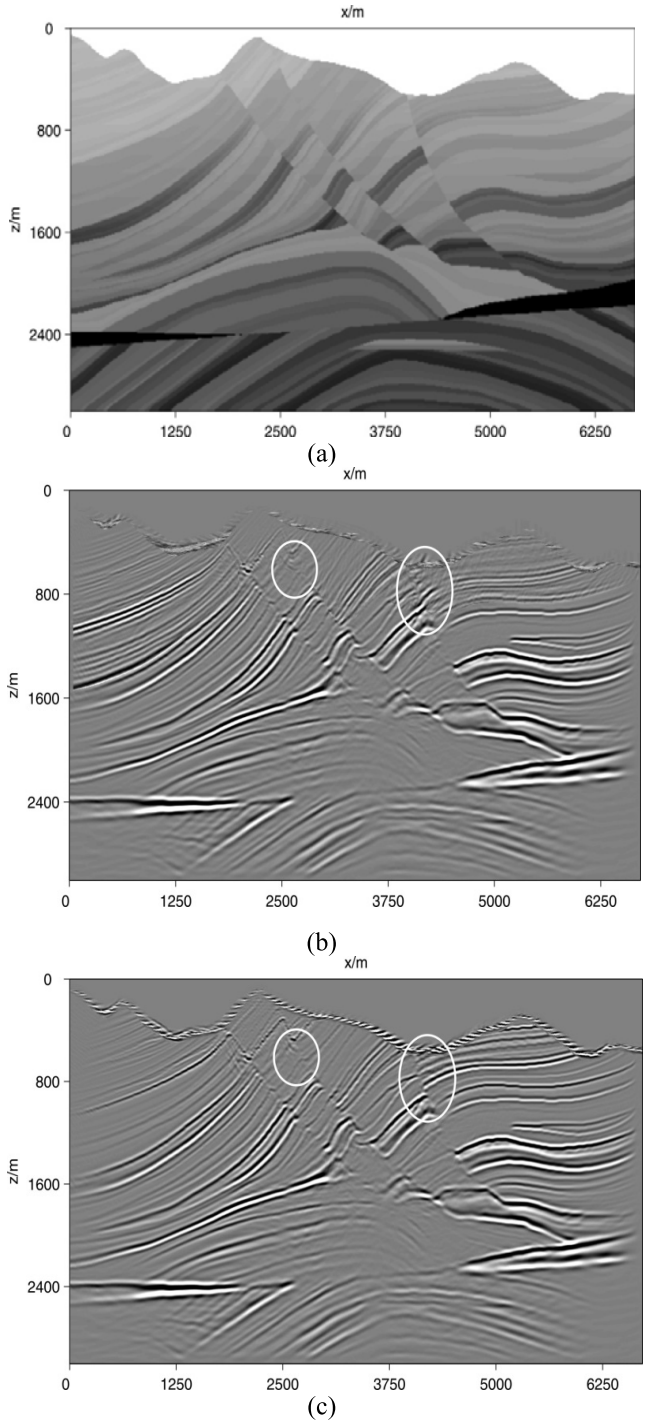

FIGURE 7. Migration result of Marmousi model, (a) velocity of Mamousi model, (b) migration result of KBM, (c)migration result of CS-KDFBM.

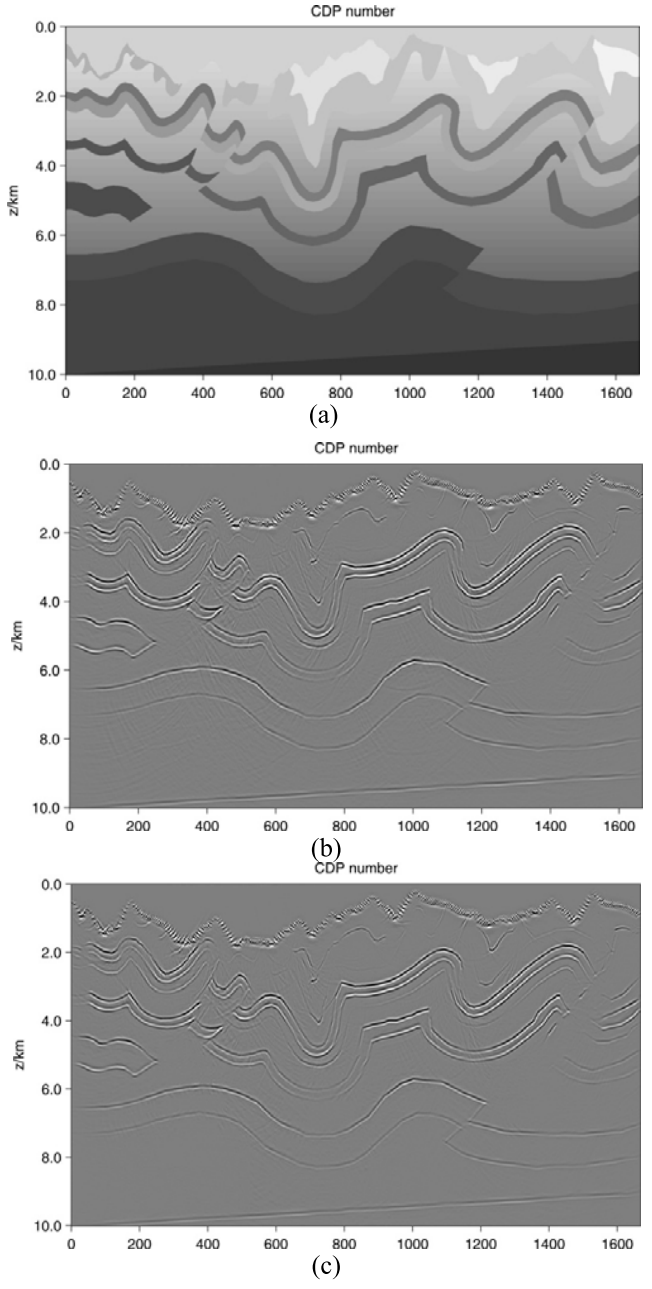

FIGURE 8. Migration result of Canadian foothills model, (a) velocity of Canadian foothills model, (b) migration result of KBM, (c)migration result of CS-KDFBM.

III. EXPERIMENTS AND ANALYSIS

This part employs Maoumousi model under topography and Canadian Foothills model to test the topographic CS-KDFBM. Marmousi model and Canadian Foothills model are both very complex models. They contain multiple faults, complex curved interfaces, and large anticlines. If the new method can get good experimental results on the two model data sets, good experimental results also could be obtained for other simple models.

Fig. 7a is the Marmousi model under topography, whose model size is 737 in the x dimension and 750 in the z dimension; grid spacing is 12.5 m in the x dimension and 4 m in the z direction. The data set has 240 shots with a fixed shot interval of 90 m. Every shot consists of 101 traces and the receiver spacing is 25m. The sampling interval in the trace is 4 ms and the recording time is 3.2 s. The offset ranges from 0 m to 2500 m. Fig. 7b and Fig. 7c are respectively the imaging results of KBM and CS-KDFBM. The two methods

adopted the same migration parameters. The ray angles in beam migrtion could be chosen from −90° to +90°. However, it is not the larger the range of rays, the better. Too large the range of rays will bring more migration noise, which will affect the final imaging result. The ray angles in these two methods range from −50° to +50° [13], [26] with a ray quantity of 25 in every launch position.

It can be found that in the shallow part of the model, the image produced by CS-KDFBM has higher signal-noise ratio and reflects clearer geological structures, especially for the fault structures in the white circle. The reason for the differences is that dynamic focused beam can guarantee the coverage of the beam in the shallow part of the model.

Fig. 8a is the Canadian Foothills model, whose model size is 1668 in the x dimension and 1000 in the z dimension; grid spacing is 15 m in the x dimension and 10 m in the z direction. The data set has 277 shots with a fixed shot interval of 90 m. The number of traces of each shot ranges from 238 to 480 and the receiver spacing is 15 m. Every trace consists of 2000 sampling points with a sampling interval of 4 ms. The minimum and maximum offset are respectively 15 m and 3600 m. Fig. 8b and Fig. 8c are respectively the imaging results of KBM and CS-KDFBM. It can be found that CS-KDFBM produced a clearer image with less migration artifact. The reasons for the differences are that CS-LRT enhances the accuracy of the local plane decomposition and the dynamic focused beam propagator controls the beam width in the deep part of the model.

IV. CONCLUSIONS

This paper studies the Kirchhoff beam migration method under irregular topography. In order to solve the problems existing in local plane wave decomposition and beam propagator, CS-LRT and dynamic focused beam propagator are introduced into KBM. The new imaging method was successfully applied to complex models (Marmousi model and Canadian Foothills model), and could obtain better images compared to the original method. CS-LRT improves the accuracy of the acquired plane waves and the anti-noise ability of the imaging method. The dynamic focused beam propagator increases the coverage of the beam in the shallow layer of the model and helps to control the beam width.

ACKNOWLEDGMENT

The authors would like to thank Prof. Sun Jianguo, Prof. Sun Zhangqing, Prof. Han Fuxing and Prof. Gong Xiangbo in Jilin University for their kindness help.

REFERENCES

[1] O. Yilmaz, *Seismic Data Analysis: Processing, Inversion and Interpretation of Seismic Data*. Tulsa, OK, USA: SEG, 2001.
[2] R.-S. Wu and M. N. Toksöz, "Diffraction tomography and multisource holography applied to seismic imaging," *Geophysics*, vol. 52, no. 1, pp. 11–25, 1987.
[3] X. Wang, J. Li, and Q.-F. Chen, "Topography of the 410 km and 660 km discontinuities beneath the Japan Sea and adjacent regions by analysis of multiple-ScS waves," *J. Geophys. Res-Solid Earth*, vol. 122, no. 2, pp. 1264–1283, Feb. 2017.
[4] Y.-G. Sun, H.-Y. Qiang, J.-Q. Xu, and D.-S. Dong, "The nonlinear dynamics and anti-sway tracking control for offshore container crane on a mobile harbor," *J. Marine Sci. Technol.*, vol. 25, no. 6, pp. 656–665, 2012.
[5] H. Sun *et al.*, "Research into the effects of seawater velocity variation on migration imaging in deep-water geology," *Earth. Sci. Res. J.*, vol. 20, no. 3, pp. H1–H7, Sep. 2016.
[6] X. Wang, K. E. Bradley, S. Wei, and W. Wu, "Active backstop faults in the Mentawai region of Sumatra, Indonesia, revealed by teleseismic broadband waveform modeling," *Earth. Planet. Sci. Lett.*, vol. 483, pp. 29–38, Feb. 2018.
[7] H. Sun *et al.*, "Synthetic Anaysis of model smoothing's influence on ray path, traveltime and migration imaging," *Appl. Ecol. Environ. Res.*, vol. 15, no. 3, pp. 443–452, Sep. 2017.
[8] K. Cui and T. T. Zhao, "Unsaturated dynamic constitutive model under cyclic loading," *Cluster Comput.*, vol. 20, no. 4, pp. 2869–2879, 2017.
[9] X. Wang, S. Wei, and W. Wu, "Double-ramp on the main himalayan thrust revealed by broadband waveform modeling of the 2015 Gorkha earthquake sequence," *Earth Planet. Sci. Lett.*, vol. 473, pp. 83–93, Sep. 2017.
[10] N. Bleistein, J. K. Cohen, and J. W. Stockwell, Jr., *Mathematics of Multi-dimensional Seismic Imaging, Migration, and Inversion*. Berlin, Germany: SSBM, 2013.
[11] J. Sun, "The history, the state of the art and the future trend of the research of kirchhoff-type migration theory: a comparison with optical diffraction theory, some new results and new understanding, and some problems to be solved," *J. Jin. Univ.*, vol. 42, no. 5, pp. 1521–1552, 2012.
[12] Z. C. Li, "Research status and development trends for seismic migration technology," *Oil. Geophys. Prospecting*, vol. 49, no. 1, pp. 1–21, 2014.
[13] N. R. Hill, "Gaussian beam migration," *Geophysics*, vol. 55, no. 11, pp. 1416–1428, Nov. 1990.
[14] D. Hale, "Migration by the Kirchhoff, slant stack, and Gaussian beam methods," CSM, Livonia, MI, USA, Tech. Rep. CWP-126, 1992.
[15] D. Hale, "Computational aspects of Gaussian beam migration," CSM, Golden, CO, USA, Tech. Rep. CWP-127, 1992.
[16] N. Hill, "Prestack Gaussian-beam depth migration," *Geophysics*, vol. 66, no. 4, pp. 1240–1250, Apr. 2001.
[17] R. L. Nowack, M. K. Sen, and P. L. Stoffa, "Gaussian beam migration for sparse common-shot and common-receiver data," in *Proc. SEG Int. Annu. Met.*, Houston, TX, USA, 2003, pp. 1114–1117.
[18] S. H. Gray, "Gaussian beam migration of common-shot records," *Geophysics*, vol. 70, no. 4, pp. S71–S77, Apr. 2005.
[19] C.-O. Ting and D. Wang, "Controlled beam migration—Application in gulf of Mexico," in *Proc. 11th Int. Congr. Brazilian Geophys. Soc.*, 2009, pp. 368–372.
[20] J. W. C. Sherwood *et al.*, "3D beam prestack depth migration with examples from around the world," *Lead. Edge*, vol. 28, no. 9, pp. 1120–1127, Sep. 2009.
[21] S. H. Gray and N. Bleistein, "True-amplitude Gaussian-beam migration," *Geophysics*, vol. 74, no. 2, pp. S11–S23, Mar. 2009.
[22] N. Bleistein and S. H. Gray, "Amplitude calculations for 3D Gaussian beam migration using complex-valued traveltimes," *Inverse Problems*, vol. 26, no. 8, p. 085017, 2010.
[23] Y. Zhang, S. Xu, N. Bleistein, and G. Zhang, "True-amplitude, angle-domain, common-image gathers from one-way wave-equation migrations," *Geophysics*, vol. 72, no. 1, pp. S49–S58, Jan. 2007.
[24] M. M. Popov, N. M. Semtchenok, P. M. Popov, and A. R. Verdel, "Depth migration by the Gaussian beam summation method," *Geophysics*, vol. 75, no. 2, pp. S81–S93, Feb. 2010.
[25] X. Huang, H. Sun, and J. Sun, "Born modeling for heterogeneous media using the Gaussian beam summation based green's function," *J. Appl. Geophys.*, vol. 131, pp. 191–201, Aug. 2016.
[26] J. Liu and G. Multiarrival, "Multiarrival Kirchhoff beam migration," *Geophysics*, vol. 76, no. 5, pp. WB109–WB118, May 2011.
[27] J. Liu and C. Marcinkovich, "Shot-profile Kirchhoff beam migration," in *Proc. SEG Annu. Met.*, Houston, TX, USA, 2013, pp. 3969–3973.
[28] J. Sun and X. Shi, "Depth migration by the delta packet summation method," in *Proc. SEG Annu. Met.*, Dallas, TX, USA, 2016, pp. 4321–4325.
[29] X. Shi, S. Jian-Guo, S. Hui, L. Ming-Chen, and L. Zhi-Qiang, "The time-domain depth migration by the summation of delta packets," *Chin. J. Geophys.*, vol. 59, no. 7, pp. 2641–2649, Jul. 2016.
[30] H. Sun *et al.*, "Joint 3D traveltime calculation based on fast marching method and wavefront construction," *Appl. Geophys.*, vol. 14, no. 1, pp. 56–63, Mar. 2017.

[31] X. Huang, J. Sun, and Z. Sun, "Local algorithm for computing complex travel time based on the complex eikonal equation," *Phys. Rev. E, Stat. Phys. Plasmas Fluids Relat. Interdiscip. Top.*, vol. 93, no. 4, p. 043307, 2016.
[32] X. Huang and S. Greenhalgh, "Linearized formulations and approximate solutions for the complex eikonal equation in orthorhombic media and applications of complex seismic traveltime," *Geophysics*, vol. 83, no. 3, pp. C115–C136, 2018.
[33] X. Huang, J. Sun, and S. Greenhalgh, "On the solution of the complex eikonal equation in acoustic VTI media: A perturbation plus optimization scheme," *Geophys. J. Int.*, vol. 214, no. 2, pp. 907–932, 2018.
[34] Y. Yue, Z.-C. Li, P. Zhang, X.-F. Zhou, and N. Qin, "Prestack Gaussian beam depth migration under complex surface conditions," *Appl. Geophys.*, vol. 7, no. 2, pp. 143–148, Jun. 2010.
[35] Y. Yue, "Amplitude-preserved Gaussian beam migration under complex topographic conditions," *Chin. J. Geophys-CH.*, vol. 55, no. 4, pp. 1376–1383, 2012.
[36] J.-D. Yang, J. P. Huang, X. Wang, Z. C. Li, and X. Y. Duan, "Prestack Fresnel beam migration method under complex topographic conditions," *Chin. J. Geophys. Ed.*, vol. 58, no. 10, pp. 3758–3770, Oct. 2015.
[37] C. Hu and P. L. Stoffa, "Slowness-driven Gaussian-beam prestack depth migration for low-fold seismic data," *Geophysics*, vol. 74, no. 6, pp. WCA35–WCA45, Nov. 2009.
[38] J. D. Yang, J. P. Huang, X. Wang, Z. C. Li, and Y. Yang, "Data-driven Gaussian beam migration based on local similarity analysis," in *Proc. 77th EAGE Conf. Exhib.*, 2015, pp. 1380–1384.
[39] B. Wu, Z. Zhu, H. Yang, and A. Osen, "High resolution beam forming for 3D common offset Kirchhoff beam migration," in *Proc. SEG Annu. Met.*, Houston, TX, USA, 2014, pp. 3837–3841.
[40] X. Gong, S. Wang, and T. Zhang, "Velocity analysis using high-resolution semblance based on sparse hyperbolic radon transform," *J. Appl. Geophys.*, vol. 134, pp. 146–152, Nov. 2016.
[41] J. Wu, S. Guo, J. Li, and D. Zeng, "Big data meet green challenges: Big data toward green applications," *IEEE Syst. J.*, vol. 10, no. 3, pp. 888–900, Sep. 2016.
[42] J. Wu, Y. D. Zhang, M. G. Amin, and M. Uysal, "Multiple-relay selection in amplify-and-forward cooperative wireless networks with multiple source nodes," *EURASIP J. Wireless Commun. Netw.*, p. 256, Dec. 2012.
[43] J. Peng and Y. Shao, "Intelligent method for identifying driving risk based on V2V multisource big data," *Complexity*, Apr. 2018, Art. no. 1801273.
[44] B. Wu, H. Yang, Z. Zhu, and A. Osen, "Local slant stack Kirchhoff common offset beam migration: Application to the SEAM model," in *Proc. SEG Annu. Met.*, Dallas, TX, USA, 2015, pp. 4283–4287.
[45] W. Hua-Zhong, F. Bo, L. Shao-Yong, H. Jiang-Tao, W. Xiong-Wen, and L. Hui, "Characteristic wavefield decomposition, imaging and inversion with prestack seismic data," *Chin. J. Geophys. Ed.*, vol. 58, no. 6, pp. 2024–2034, Jun. 2015.
[46] H. Wang, B. Feng, and X. Wang, "Compressed sensing and its application in seismic exploration," *Geophys. Prospecting Petroleum*, vol. 55, no. 4, pp. 467–474, Apr. 2016.
[47] S. Liu, H. Wang, and B. Feng, "The characteristic wave decomposition and imaging in VTI media," *J. Appl. Geophys.*, vol. 115, pp. 51–58, Apr. 2015.
[48] H. Sun *et al.*, "Kirchhoff beam migration based on compressive sensing," *IEEE Access*, vol. 6, pp. 26520–26529, 2018.
[49] V. Červený, M. M. Popov, and I. Pšencík, "Computation of wave fields in inhomogeneous media—Gaussian beam approach," *Geophys. J. Roy. Astronomical Soc.*, vol. 70, no. 1, pp. 109–128, Jan. 1982.
[50] H. Sun and G. T. Schuster, "2-D wavepath migration," *Geophysics*, vol. 65, no. 5, pp. 1528–1537, 2001.
[51] R. Nowack, "Focused Gaussian beams for seismic imaging," in *Proc. SEG Int. Annu. Met.*, Las Vegas, NV, USA, 2008, pp. 2376–2380.
[52] R. L. Nowack, "Dynamically focused Gaussian beams for seismic imaging," *Int. J. Geophys.*, vol. 2011, Mar. 2011, Art. no. 316581.
[53] J.-D. Yang, J.-P. Huang, X. Wang, and Z.-C. Li, "An amplitude-preserved adaptive focused beam seismic migration method," *Petroleum Sci.*, vol. 12, no. 3, pp. 417–427, 2015.
[54] X. Xiao, F. Hao, C. Egger, B. Wang, F. Jiao, and X. Wang, "Final laser-beam Q-migration," in *Proc. SEG Int. Annu. Met.*, Beijing, China, 2014, pp. 3872–3876.
[55] X. Xiao *et al.*, "Orthorhombic control laser beam migration," in *Proc. SEG Int. Annu. Met.*, Beijing, China, 2014, pp. 3857–3861.
[56] J. Huang, J. Yang, W. Liao, X. Wang, and Z. Li, "Common-shot Fresnel beam migration based on wave-field approximation in effective vicinity under complex topographic conditions," *Geophys. Prospecting*, vol. 64, no. 3, pp. 554–570, 2016.
[57] V. Červený *et al.*, *Ray Method in Seismology*. Prague, Czech Republic: Univ. Karlova, 1977.

HUI SUN received the B.S. and Ph.D. degrees in geophysics from Jilin University, China, in 2011 and 2017, respectively. He is currently a Lecturer with the Faculty of Geosciences and Environmental Engineering, Southwest Jiaotong University. His research interests include seismic signal processing, seismic imaging methods, and forward modeling.

FEILONG YANG received the B.S. and M.S. degrees in geophysical prospecting from Xi'an Shiyou University in 2010 and 2013, respectively, and the Ph.D. degree in geophysical prospecting from Chang'an University, China, in 2016. He is currently a Lecturer with the School of Earth Sciences and Engineering, Xi'an Shiyou University, China. His research interests include seismic data processing, seismic wave field numerical modeling, and migration imaging.

FANCHANG MENG received the B.S. and M.S. degrees in geophysics from Jilin University, China, in 2011 and 2014, respectively. He is currently pursuing the Ph.D. degree in seismology with the Institute of Geology and Geophysics, Chinese Academy of Science. He was with the Chinese Railway Design Corporation from 2014 to 2017. His research interests include seismology, receiver functions, and migration images.

ZHIHOU ZHANG received the B.S. and M.S. degrees in geophysics from Jilin University in 2005 and 2007, respectively, and the Ph.D. degree in geophysics from Zhejiang University, China, in 2013. He is currently a Lecturer with the Southwest Jiaotong University, China, His research interests include signal processing in geophysics.

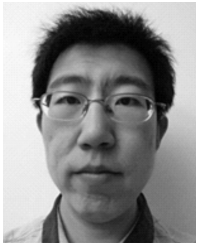

CHENG GAO received the B.S. degree in applied geophysics and the Ph.D. degree in geodetection and information technology from Jilin University, China, in 2008 and 2015, respectively. He is currently a Lecturer with the School of Mines, Inner Mongolia University of Technology, China. His research interests include seismic signal processing and migration imaging.

MINGCHEN LIU received the B.S. degrees in geophysics from Jilin University, China, in 2011, where he is currently pursuing the Ph.D. degree in geophysics. His research interests include seismology, receiver functions, and seismic migration.